



International Journal of Nanotechnology

ISSN online: 1741-8151 - ISSN print: 1475-7435

<https://www.inderscience.com/ijnt>

Dimension adaptive hybrid recovery with collaborative group sparse representation based compressive sensing for colour images

Abhishek Jain, Preety D. Swami, Ashutosh Datar

DOI: [10.1504/IJNT.2022.10052022](https://doi.org/10.1504/IJNT.2022.10052022)

Article History:

Received:	25 November 2021
Last revised:	06 May 2022
Accepted:	16 May 2022
Published online:	31 May 2023

Dimension adaptive hybrid recovery with collaborative group sparse representation based compressive sensing for colour images

Abhishek Jain*

Department of Electrical and Electronics Engineering,
Samrat Ashok Technological Institute,
Vidisha (MP), 464001, India
Email: abhishekjain.ec@satiengg.in

*Corresponding author

Preety D. Swami

Department of Electronics and Communication Engineering,
UIT,
RGPV Bhopal (MP), 462033, India
Email: preetydswami@gmail.com

Ashutosh Datar

Department of Electrical and Electronics Engineering,
Samrat Ashok Technological Institute,
Vidisha (MP), 464001, India
Email: ashutoshdatar.bme@satiengg.in

Abstract: In this paper, a fast and efficient hybrid method of image compressive sensing (termed as HRCoGSR) is designed which can adaptively acquire grey or colour image and can faithfully recover it speedily. The proposed method combines and utilises the approaches of recovery via collaborative sparsity (RCoS) and group sparse representation (GSR). For fast convergence, Gaussian Pyramid (GP) is constructed at the front-end and then block compressive sensing (BCS) based RCoS recovery is applied. In the second phase, restricted GSR process is carried out for further enhancing the perceptual quality. The collaborative sparsity-based CS solution is an iterative method and intends to improve signal-to-noise ratio (SNR) performance of the recovered image. It simultaneously enforces local 2D and 3D non-local sparsity in adaptive hybrid transform domain. Parametric performance of the proposed HRCoGSR method is tested over variety of standard grey and colour images and compared with seven existing state-of-the-art methods. Experimental results show that the proposed HRCoGSR method is highly efficient and much faster than existing methods. The average computational time taken by the proposed method is only 26% of that of the standard RCoS method and 46% of the GSR method.

Keywords: compressive sensing; RCoS; recovery via collaborative sparsity; GSR; group sparse representation; hybrid recovery; Gaussian pyramid; adaptive colour image compression; collaborative recovery; image acquisition.

Reference to this paper should be made as follows: Jain, A., Swami, P.D. and Datar, A. (2023) 'Dimension adaptive hybrid recovery with collaborative group sparse representation based compressive sensing for colour images', *Int. J. Nanotechnol.*, Vol. 20, Nos. 1/2/3/4, pp.361–389.

Biographical notes: Abhishek Jain is pursuing PhD in Electronics and Communication Engineering from Rajiv Gandhi Proudyogiki Vishwavidyalaya, Bhopal, India. He received his Master's degree in Digital Communication from Barkatullah University, Bhopal, India (2011) and received Bachelor's degree in Electronics and Communication Engineering from Rajiv Gandhi Proudyogiki Vishwavidyalaya, Bhopal, India (2007). He has qualified GATE (in Electronics and Communication Engineering) four times and has certification in CCNA. He is also a NASSCOM certified trainer in IT-ITeS Sector approved by National Skill Development Council. He is having 15 years of teaching and research experience. He has 15 research publications in national and international journals/conferences. He is a Lifetime Member of Institution of Electronics and Telecommunication Engineers (IETE) since 2012. His research orients towards digital image processing, digital communication and computer networking. He is currently working as an Assistant Professor in Department of Electronics Engineering, Samrat Ashok Technological Institute, Vidisha, India.

Preety D. Swami received her BE in Electronics and Instrumentation Engineering from Samrat Ashok Technological Institute, Vidisha, India in 1992; MTech in Digital Communication from MANIT, Bhopal, India in 2008 and PhD in Electronics Engineering from RGPV, Bhopal, India in 2013. She is currently working as a Professor at the Department of Electronics and Communication Engineering, UIT, RGPV, Bhopal. Her research interests include digital signal processing and digital image processing.

Ashutosh Datar received his BE (Electronics and Instrumentation Engineering) from Samrat Ashok Technological Institute, Vidisha (MP) India, and MTech (Biomedical Engineering) from Institute of Technology, Banaras Hindu University (Now IIT BHU) Varanasi, in 1989 and 1998, respectively. He obtained his Doctoral degree from Rajiv Gandhi Proudyogiki Vishwavidyalaya, Bhopal India in 2012. He is presently working as Professor in Department of Electrical and Electronics Engineering, Samrat Ashok Technological Institute, Vidisha (MP) India. He is a Life Member of IE(I), ISTE, BMESI, Instrumentation Society of India. His current research interests include DSP, multirate signal processing, filterbanks, biosignal processing, medical image processing, AI and machine learning.

1 Introduction

With advancements in social media and IoT based vision applications, huge capacity of imaging data is trafficked or uploaded over the web servers on daily basis. Storing and recovery of imaging data is always a challenge in several contexts along with limited hardware and power constrained sensors. Additionally, a lot of bandwidth and time is required for transmitting the images wirelessly. So, it is essential to look for an efficient and fast compression technique. Over the last decade, compressive sensing (CS) [1–6]

based recovery methods have gained lot of popularity due to its dimensional reduction features. It is primarily a combination of encoding and decoding methodologies that mingle sampling and compression. CS based methods exploit the redundancy which exists in a signal. CS theory demonstrates that a signal can be faithfully reconstructed with high probability when it exhibits sparsity in some domain. As most of the images are sparse in nature, therefore they can be decoded using the CS concept with fewer samples even much fewer than the Shannon's Theorem/Nyquist Rate. Conventional sampling methods acquire hi-fidelity signal/images using costlier sensors and devices which are then followed by lossy compression methods. On the other hand, CS based methods merge the data acquisition process along with sparse compression. The research goal in this domain is to reduce the memory requirement and the quality of recovered image from the CS based encoding. It is also required to minimise the overall computational time and the complexity of the optimisation [3] solved to recover (decode) the images back at the receiver end. The conventional methods of CS based image recovery [1–4] have exploited the fixed set of transforms viz. wavelet or DCT along with gradient descent search methods. There have been many methods proposed in literature for improving the efficiency of CS for image compression and recovery.

Mun and Fowler [2] proposed a directional transformation method of CS using Block compressive sensing (BCS). Authors utilise the dual tree wavelet transform for directional features. Reconstruction is achieved through Wiener filter based Smoothing with Projected Landweber (SPL). This technique outperforms other pursuit-based methods in terms of recovery and image quality. However, it is computationally complex and expensive [7,8].

A very impressive and efficient CS method – recovery via collaborative sparsity (RCoS) [3] was proposed by Zhang et al. CS recovery is done by collective sparsity, utilising the benefits of both nearby 2D sparsity and non-local 3D sparsity constraints. It is one of the hardest re-look in CS techniques. The method outperformed tree structured wavelet (TSW) CS method [4] and tree-structured CS with variational Bayesian analysis using DCT (TSDCT) approach [5]. Only concern of this RCoS method is higher computational time as it exploits Gradient descent approach for non-local sparsity.

Zhang et al. [6] proposed one more technique of CS recovery by adaptively learning the basis of sparsity using the minimisation through l_0 optimisation problem. Using the adaptively picked up sparse basis in the type of l_0 standard, the authors addressed the inadequately covered image patches and achieved the intrinsic local sparsity of images. For efficient results, the authors built an approach based on split Bregman cycle for efficiently managing a non-arched l_0 based minimisation problems.

Various total variation (TV) based approaches were also proposed in [9–11]. The total variation based minimisation using the augmented Lagrangian [12,13] with combination of approach of alternating direction algorithm (TVAL3) is proposed in [9]. An improved approach of the total variation is implemented by Li et al. [10] which utilises the non-local means (NLM) based smoothing and the image self-similarities. Use of NLM based smoothing has been found effective to preserve and sharpen the edges in images. This method has proven effective to eliminate the staircase effects in images. TVNLR method by Zhang et al. in [11] utilised non-local regularisation for implementing the CS. But still the overall reconstruction quality and the similarity measure performance needs to be improved. In [14,15], BCS is combined with Split Bregman based approach for achieving high visual recovery performance. Chen et al. [16] created a hybrid method by combining fractional-order TV method and sparsifying

transformations. Zhong et al. in [17] designed block based CS recovery method by reweighting sparsity constraints.

Zhang et al. [18] proposed another system where image sparsity and image self-closeness are imposed under a joint system in an adaptable arrangement space. It leads to higher convergence of CS solution. Several methods based on multi-hypothesis [MH] approach are also proposed in [19–21], where MH is used as reconstruction initialisation in CS recovery.

Sparse patch-based illustration takes more time in the optimisation phase. Hence, in place of patch, set of non-local patches called ‘group’ is measured as the essential unit of sparse representation in [22]. It leads to a new representation form of images known as Group based sparse representation (GSR). In the past few years, several GSR based algorithms including Joint Patch based GSR algorithms of CS were proposed [23–29] which are widely used for performance improvement. Shi et al. [23,24] expanded the use of GSR on low lighting and remote sensing images. Zha et al. [25] developed a combined patch group representation for image in painting. Xu et al. [26] united GSR and non-local TV approach to enhance the optimisation of image CS recovery. Xie et al. [27] proposed an entropy-based calculation that leads to higher image sparsity through the knowledge of group sparsity of residual. Li et al. [28] proposed a CS system based on GSR model that leads to a non-convex non-smooth low-position minimisation problem. M-estimator and the famous l_2 -norm are utilised for faithful image CS recovery. For the removal of additional shrinking issue, a group of nuclear norms are used here. Zha et al. [29] proposed a new joint patch-group GSR algorithm to overcome the artefacts and over-smoothing issues of patch and group sparse methods. Different variants of CS are also proposed on various perspectives such as less complex kernel regression for image recovery [30], non-local CS [31], adaptive BCS [32], Robust adaptive learning of dictionary pairs for CS [33] etc. Erkoc et al. offered a novel method of sparse signal recovery by swarm intelligence-based technique. This approach utilises the least square technique to recover the signal [34]. A method termed as hybrid non-local sparsity regularisation (HNLSR) was presented in [35]. Authors developed a novel minimisation approach using self-generated singular value decomposition (SVD) and fixed 3D dictionaries. A fast Gaussian Pyramid based RCoS method is also presented in [36]. This method takes exceptionally low computational time compared to previous collaborative CS approaches. The only drawback is over-smoothing in bigger size images.

Due to advancement in the technologies, an effective data acquisition system is the need of the hour. Smart systems have the potential to make data-driven judgements on the basis of the acquired data from several devices. Various smart uses of data acquisition systems are presented in [37]. The bio-data acquisition systems provide major impacts in medical care, diagnostic processes and public health. CS can also be exploited to lower the data of signals like electrocardiogram (ECG), electroencephalogram (EEG) and other bio-signals. Kakaraparty et al. developed a low-power acquisition CS circuit for neural signals in [38]. The authors implemented a CMOS build interface with a new arbitrary sequence maker using the CS concept. Their work effectively reduces the power consumption per channel. A new CS based method for ultrasound images is presented in [39]. Authors achieved the sparsity of the images by Bandlet transform in this work and then image recovery is done by corresponding pursuit-based CS method.

There are several challenges faced by image CS algorithm designing. CS exploits the important property of signal/image sparsity. Thus, it is always required to get higher

degree of sparsity. Another major challenge is to limit the higher computation time during reconstruction. Selection of projection template is also a key challenge. CS recovery is typically an image linear inverse problem, for which it has been known that image priors play a key role to achieve high-quality results. CS methods use mathematical optimisation techniques such as l_0 or l_1 for recovering original images back during decompression [6]. Another challenge is to optimise the recovery method parameters for better recovered results. Recovery time can be minimised using down sampling methods. However, selection of suitable method with higher PSNR performance and less over-flattening of images is a challenging task in hand. It is required to recover a good quality image in the presence of noise also. Most of the previous CS based methods [3,6,10] were designed for grey images or convert colour to grey before being used. Thus, designing an efficient CS based method that can efficiently work for both grey and colour image is required.

1.1 Contribution of the proposed work

- The work proposes a very fast and efficient hierarchical pyramid based novel image CS method (termed as HRCoGSR) which can adopt both grey and colour images of different dimensions.
- Results clarify that the proposed method has tremendous dominance over other standard methods in terms of computational time and PSNR performance.
- Several other groundwork experiments are also carried out, such as:
 - i performance evaluation of uniform random distribution (URD) and ortho-normal random distribution (ONRD) based CS projection matrices
 - ii comparison of RGB and CIELAB colour spaces by calculating mean brightness and standard deviation of various images.
- The proposed work has been verified by experimenting it over a large number of grey and colour images for different values of measurements/sampling ratios (r).

1.2 Organisation of the paper

This section has illustrated the purpose of the research, major challenges in CS methods, literature review and contribution of the proposed work. The remaining paper is organised as follows. Section 2 describes the background of CS recovery. It introduces BCS with projected Landweber and augmented Lagrangian methods. Section 3 provides a basis of some groundwork experiments and algorithms developed to be used in the proposed work. It includes:

- i colour space representation
- ii Gaussian Pyramid construction
- iii image adoption
- iv performance evaluation of URD and ONRD based CS projection matrices.

Section 4 describes the working of the proposed HRCoGSR method along with block diagram, algorithms, and flow chart. Section 5 illustrates the parametric performance

evaluation of the proposed HRCoGSR method with several existing CS methods. Section 6 presents the conclusion and major findings of the work.

2 Background

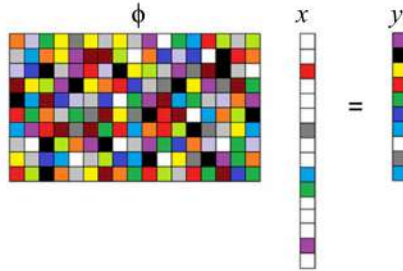
An example of single vector CS based sparse recovery method is shown in Figure 1 which can be expressed as:

$$y = \phi \times x. \tag{1}$$

where, y is the sparse signal, ϕ is the random sample vector (non-orthogonal projection matrix of image) and x is the observed measurements.

It can be observed that simple matrix operations and transformation functions can compress the signal to generate the sparse representation. The recovery from the above equation is basic BCS open problem in hand to be addressed.

Figure 1 CS approach (see online version for colours)



2.1 Block compressive sensing with SPL (BCS-SPL)

BCS-SPL is a combined arrangement of block-based compressive sensing (BCS) and smoothed-projected landweber (SPL) recovery method. In BCS, the entire image is partitioned into blocks of size $B \times B$ and sampled by a suitable measurement matrix. CS recovery of signal x of length N from an M length measurement vector y (samples) from equation $y = \phi x$ is a complicated process. Here ϕ is an $M \times N$ measurement matrix and $M \ll N$. It further leads to an underdetermined system of linear equations and will have infinite number of possible solutions. Input signal is recovered back by solving for the sparsest x that is consistent with measurement y . The basis pursuit (BP) method solves the convex l_1 optimisation problem defined as;

$$\tilde{x} = \arg \min_x \|\tilde{x}\|_1, \text{ such that, } y = \phi \phi^{-1} \tilde{x}. \tag{2}$$

where, basis function ϕ is orthonormal randomly generated projection matrix, so that it is satisfying the condition $\phi \phi^T = I$. Techniques based on projections were also proposed in the literature as this BP based solution is computationally complex. Algorithms of

successive projection with thresholding forms \tilde{x} [7], that starts from some initial approximation $\hat{x}^{(0)}$ and then the next $i + 1$ th iteration is approximated as;

$$x^{(i)} = \tilde{x}^{(i)} + \frac{1}{\gamma} \varphi \varphi^T \left(y - \varphi \varphi^{-1} \tilde{x}^{(i)} \right). \tag{3}$$

$$\tilde{x}^{(i+1)} = \begin{cases} \tilde{x}^{(i)}, & \left| \tilde{x}^{(i)} \right| \geq \tau^{(i)} \\ 0 & else \end{cases}. \tag{4}$$

The above process is an example of projected Landweber (PL) algorithm [8], parameter γ is a scaling factor which considers the largest Eigen values of matrix $(\varphi \varphi^T)$ and $\tau^{(i)}$ is a set suitable threshold at each iteration. In SPL, Wiener filtering was included that apart from sparsity helps in attaining smoothness. In the research work, BCS-SPL algorithm is used and sparse measurements ($y = \hat{x}^{(i)}$) are generated using block size $B = 32 \times 32$.

2.2 Augmented Lagrangian method

A major strength of BCS based image compression is that its encoder is independent of the image signal and is less computationally complex [2,3,14]. As a specific advantage during CS based encoding, the same random projection can be applied on all input images, and it does not depend on any differences in image features. But simultaneously the CS decoders are computationally highly complex. Usually, the complex optimisation problem is solved at the decoder for recovering randomly sampled image data in a sparse domain [3].

The CS approach can be considered as the constrained optimisation problem which can be mathematically defined as;

$$\min_f E(f), \quad \text{such that,} \quad Hf = g. \tag{5}$$

For the case of m linear equality constraints, the function f, g and H are defined as subset of the

$$f \in R^n, \quad g \in R^m, \quad H \in R^{m \times n}. \tag{6}$$

The solution to the constrained optimisation by the Augmented Lagrangian Function (ALF) as referred by Jian [3] is expressed as;

$$\mathcal{L}_A(f, \lambda) = E(f) - \lambda^T (Hf - g) + \frac{\mu}{2} \|Hf - g\|_2^2. \tag{7}$$

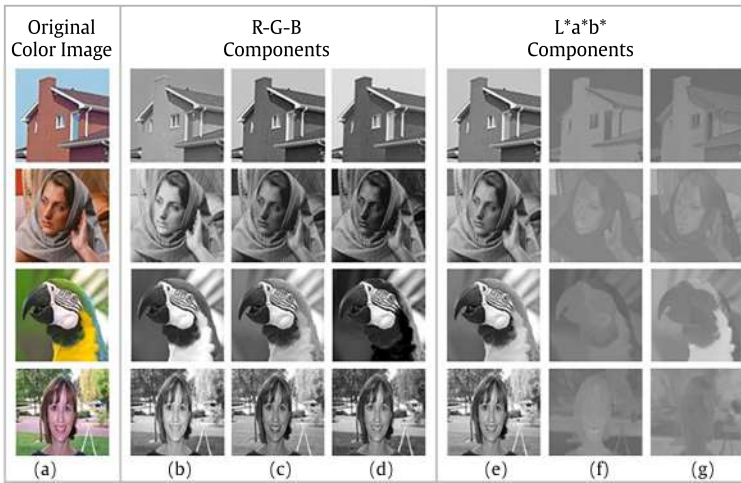
where, λ is Lagrangian multipliers vector and $\lambda \in \mathbb{R}^m$ and $\mu \geq 0$ as referred in [12,13]. Idea behind this methodology is to determine the optimum saddle point for ALF function $\mathcal{L}_A(f, \lambda)$, which fits as a solution for constrained optimisation problem given in equation (7).

3 Background

3.1 Colour space representation

In this paper, true colour images are converted to CIELAB ($L^*a^*b^*$) colour space [40]. In this 3-dimensional colour space, L^* represents the perceptual lightness. a^* and b^* are colour channels representing four distinctive colours of vision. Comparison of $L^*a^*b^*$ colour space with RGB colour space for different colour images is shown in Figure 2. It can be clearly observed that L^* component gives better visual representation than RGB components. Perceptual quality of L^* component is evidently noticed for the House and Barbara images in Figure 2.

Figure 2 RGB and CIELAB ($L^*a^*b^*$) colour space representation: (a) original colour image; (b)–(d) R-G-B components and (e)–(g) $L^*a^*b^*$ components respectively (see online version for colours)



Mean brightness and standard deviation of various images are calculated for RGB and CIELAB colour spaces and is presented in Table 1. On the basis of these parameters, it is evident that CIELAB offers better colour representation than RGB. But similar to RGB colour space, CIELAB space also requires that input image should be a 3D matrix. CIELAB space has a decoupling property between intensity and colour which is required for adoption of 2D grey and 3D colour images for our adaptive model. Thus, this paper proposes to adopt this image dimension in front-end of algorithm.

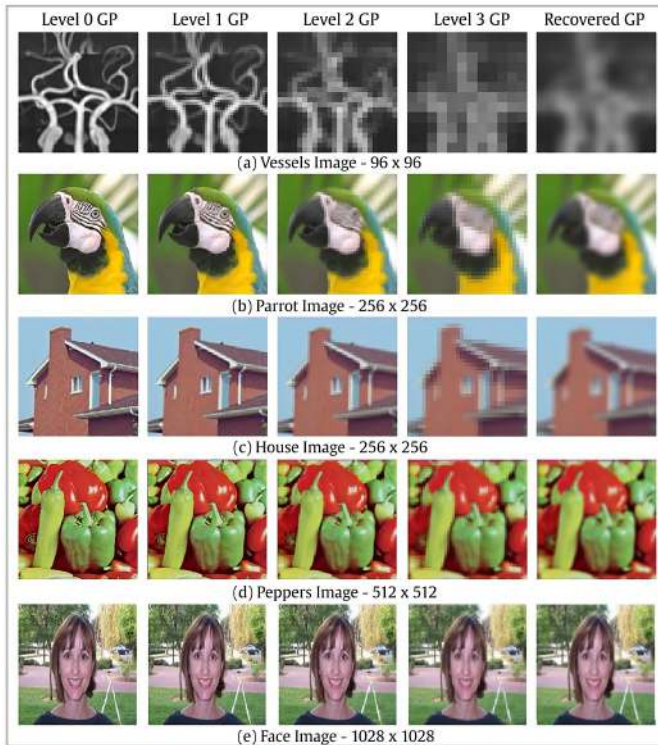
Table 1 Mean brightness and standard deviation analysis of various images for RGB and CIELAB colour spaces

Parameters	Colour space	Images				
		House	Barbara	Parrot	Face	Peppers
Standard Deviation	RGB	52.21	55.39	69.48	54.56	66.18
	CIELAB	31.02	31.62	39.24	32.30	40.13
Mean Brightness	RGB	140.53	113.19	119.44	130.40	110.64
	CIELAB	136.23	135.11	138.05	136.07	145.83

3.2 Gaussian pyramid construction

Most of the existing CS based recovery methods are computationally complex and time consuming. Thus, it is required to design an efficient and faster approach of CS based image recovery. The intended solution is to construct a Hierarchical Gaussian pyramid and then recover the image at a lower size. The major challenge in this approach is to select the suitable image pyramid method. Observationally, it has been found that due to down sampling of images most of image pyramid-based methods are sensitive to over smoothing and may cause blurry images after reconstruction. Figure 3 illustrates the Gaussian Pyramid construction for distinct images of different sizes up to level-3 decomposition. It clearly depicts that after certain number of decomposition levels, input images get blurred. Blurriness further increases with number of levels. This is because of over-smoothing of image during pyramid constructions. So, it is highly required to optimally select the number of pyramid levels. Therefore, in this paper, a fuzzy based pyramid formation algorithm is used [36]. Empirically, optimum fuzzy set of rules are formulated for limiting the pyramid levels as mentioned in Theorem 1.

Figure 3 Blurriness effect in GP construction for different image sizes (see online version for colours)



3.2.1 Theorem 1

The image pyramid decomposition levels L_p must be optimally set on the basis of the maximum image size S_{max} . The optimal level is subjected to

$$L_{opt} = \left\| \frac{S_{max}}{M} \right\|_{roundup} . \tag{8}$$

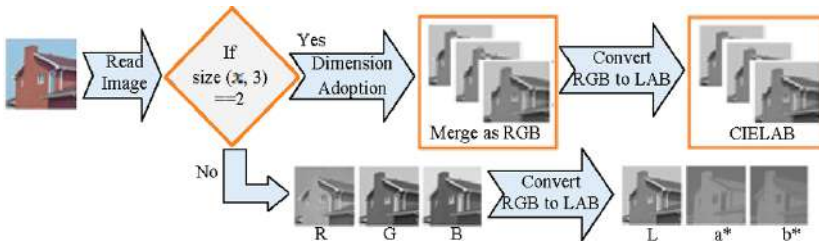
Here, M is 2^8 and L_{opt} is the optimal level of the pyramid.

3.3 3-Dimension image adoption

Most of the previous CS methods have evaluated their performance over 2D grey images only or by converting colour image to grey image before compression. These methods were computationally expensive and huge memory space is required to store random sampling data. There must be a compromise between the speed of the algorithm and its efficiency.

In this paper, a novel colour image compression method is designed which works equally well for colour and grey images. This research work proposes to adopt the dimensions in 3D space, irrespective of the input image dimensions. The methodology of front-end colour image dimension adoption CS algorithm for input image is shown in Figure 4.

Figure 4 Adaptive colour space and dimension adoption algorithm (see online version for colours)



As required for CIELAB colour space, if image size is 2D then it is converted to 3D without any change. Thus, method adopts and performs well for both dimensions. The dimensional adaptive process is presented in Algorithm 1.

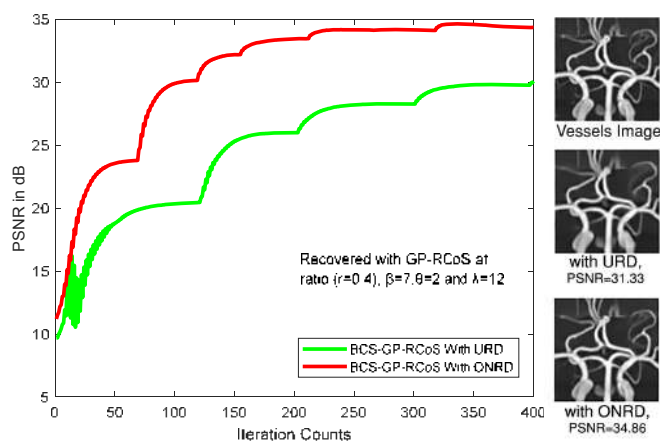
Algorithm 1 Image dimensional adoption algorithm

-
1. Acquire Input image: original color image x
 2. Calculate the image dimensions;
 3. if size $(x, 3) == 2$
 4. Convert the 2D gray image to 3D matrix.
 5. Convert RGB to CIELAB color space.
 6. end if
 7. if size $(x, 3) == 3$
 8. Convert RGB to CIELAB color spaces
-

3.4 Projection matrix

The efficiency of CS is highly dependent on the accuracy of generated compressed measurements. Selection of the projection matrix also yields noteworthy improvements in the recovery results. Therefore, in this paper, URD and ONRD based projection matrices are generated and compared. An experiment is performed for Gaussian Pyramid based RCoS (GP-RCoS) method for the projection matrices of URD and ONRD termed as BCS-GP-RCoS-URD method and BCS-GP-RCoS-ONRD method respectively. PSNR values for both the methods are calculated for different iteration counts and plotted as shown in Figure 5 for Vessels image with sample measurements/sampling ratio (r) = 0.4 (i.e., 40%).

Figure 5 Comparison of uniform random distribution (URD) and ortho normal random distribution (ONRD) projection matrix for BCS-GP-RCoS (see online version for colours)



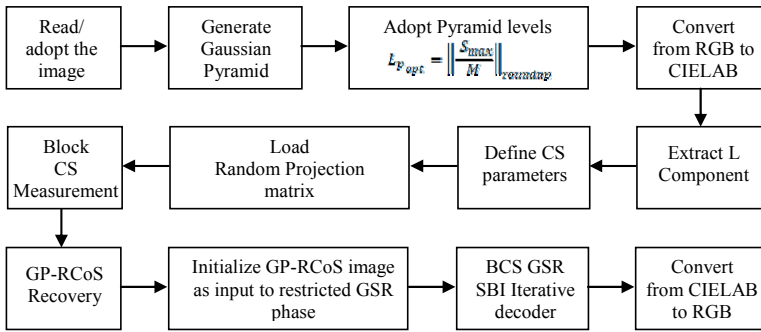
It has been observed that ONRD based projection matrix method gives higher PSNR values as compared with URD method. However, for proper comparative evaluation, it is proposed to use the same projection matrix as referred in the reference research works (In this paper, the available random projection matrix file used in [2] and [3] has been employed for relative comparison).

4 Proposed methodology

In this paper, a dimension adaptive hierarchical hybrid recovery with collaborative group sparse representation (HRCoGSR) method of image compressive sensing is developed. The proposed method utilises the characteristics of Gaussian Pyramid based Recovery with collaborative sparsity (GP-RCoS) and restricted Group Sparse Representation (GSR) approaches. Dimension adaptive algorithm as explained in Section 3.1 can adopt 2D grey and 3D colour images and work efficiently in both the cases. The hierarchical Gaussian Pyramid is constructed for down sampling the image to the appropriate level. Here, CIELAB colour space is chosen for representing the colour images for better representation which has been demonstrated in Section 3.2. This research work

contributes to optimise the collaborative sparsity methods for high speed execution and enhanced reconstruction. Collaborative sparsity simultaneously enforces local 2D and 3D non-local sparsity in adaptive hybrid transformed space [3]. GP-RCoS based CS solution is an iterative method and aims to improve the SNR performance of the recovery. However, empirically, it has been observed that GP-RCoS has a challenge in adopting image sparsity constraint and will lead to some blurriness [36]. Therefore, the recovery result of GP-RCoS is proposed to use as an input to additional restricted GSR phase. GSR opts singular value based hard threshold shrinkage approach which is implemented over group of patches. Thus, it overcomes the sparsity constraint. GP-RCoS output is cascaded with the restricted GSR model for the improvement in reconstruction quality. To implement fast convergence, restricted Split Bregman Iteration (SBI) [14,15] decoder is used in this paper. The block diagram of the proposed HRCoGSR method is shown in Figure 6. As discussed in Section 3.2, Gaussian pyramid is constructed initially which is followed by the front-end dimension adoption algorithm. Further, BCS with GP-RCoS is applied in the first phase and then the restricted GSR phase is employed by initialising the restricted GSR algorithm with GP-RCoS image as input. Finally, SBI decoder iteratively recovers the input image as shown in Figure 6.

Figure 6 Block diagram of the proposed HRCoGSR method



4.1 Gaussian pyramid based recovery via collaborative sparsity (GP-RCoS): phase 1

The method of collaborative sparsity takes advantage of local smoothness derivatives and complex non-local self-similarities [3]. In this phase, gradients are calculated for representing the local smoothness within local region, while non-local regions represent similarity of the repetitive structures or textures of the original images. Thus, a collaborative adaptive domain is achieved here; which results in a higher degree of sparsity exhibited by the image.

4.1.1 Collaborative sparsity measure (CoSM)

To achieve CS recovery of the images, a collaborative sparsity based measure (CoSM) is defined for recovering the high fidelity images back [3]. For mathematical modelling of the CS system, consider u as a sparse image matrix, A is random non-orthogonal projection matrix and b is the observed measurements with/without noise. The constrained optimisation problem will be:

$$\min_u \|\phi u\|_p, \quad \text{such that,} \quad b = Au \quad (9)$$

where, p is 1 or 0 which defines sparsity, $\|\cdot\|_1$ denotes l_1 norm and $\|\cdot\|_0$ denotes l_0 norm. The RCoS recovery uses a hybrid combination of local 2D gradients based sparsity ϕ_{L2D} in space domain and non-local 3D sparsity ϕ_{NL3D} in transform domain. The collaboration measure is represented as;

$$\text{CoSM}(u) = \phi_{L2D}(u)_p + \alpha \phi_{NL3D}(u)_q. \quad (10)$$

where, α is the parameter to control the sparsity constraints, p and q are numbers in the interval $[0, 1]$ and are set to maximum here. The 2D local sparsity ϕ_{L2D} is computed using the gradients in x and y direction denoted by D_x and D_y and articulated as

$$\|\phi_{L2D}(u)\|_1 = \|Du\|_1 = \|D_y u\|_1 + \|D_x u\|_1 \quad (11)$$

The above equation can also be referred from [9]. The non-local self-similarity is achieved by grouping similar patches for producing 3D transformation [3]. Image x is divided into n overlapped patches of size B_s and denoted by x_k where, $k = 1, 2, \dots, n$. For finding the C best similar patch, a searching window of length $L \times L$ is used and with similar image regions, a group of patches is formed which is denoted by Z_{xk} . Then, a three-dimensional operator T^{3D} is applied to obtain the coefficients in ϕ_{N3D} domain. Similar operation is performed on the entire image. The mathematical formulation of the non-local 3D sparsity of the whole image in transform domain ϕ_{N3D} is written as

$$\|\phi_{N3D} x\|_0 = \|\Theta_x\|_0 = \sum_{k=1}^n \|T^{3D}(Z_{xk})\|_0. \quad (12)$$

The estimates of all 9 blocks are averaged together for achieving the final non-local estimate expressed as $\hat{x} = \Omega_{N3D} \Theta_x$ where Ω_{N3D} is the inverse operator corresponding to ϕ_{N3D} . The collaborative sparsity measure (CoSM) can now be expressed as the combination of local and non-local 3D sparsity from equations (11) and (12) as;

$$\text{CoSM}(u) = \|\phi_{L2D}(u)\|_1 + \alpha \|\phi_{NL3D}(u)\|_0 = \|Du\|_1 + \alpha \|\Theta_u\|_0 \quad (13)$$

4.1.2 GP-RCoS recovery

Taking all the above collaborative sparsity constraints, the optimisation problem for recovery is given by:

$$\min_u \|Du\|_1 + \alpha \|\Theta_u\|_0, \quad \text{such that,} \quad Au = b \quad (14)$$

Equation (14) here is nonconvex and terribly complex to solve. Thus, it is mathematically devised by introducing supplementary variables w and x as:

$$\min_{w,u,x} \|w\|_1 + \alpha \|\Theta_x\|_0, \quad \text{such that,} \quad Du = w, \quad u = x, \quad Au = b. \quad (15)$$

The corresponding Augmented Lagrangian function (ALF) can be represented as;

$$\begin{aligned} \mathcal{L}_A(w, u, x) = & \|w\|_1 - v^T (\mathcal{D}u - w) + \frac{\beta}{2} \|\mathcal{D}u - w\|_2^2 + \gamma^T (u - x) \\ & + \frac{\theta}{2} \|u - x\|_2^2 + \frac{\mu}{2} \|Au - b\|_2^2 - \lambda^T (Au - b) \end{aligned} \quad (16)$$

There are three quadratic penalty terms in equation (16) represented as $\|\mathcal{D}u - w\|_2^2$, $\|u - x\|_2^2$ and $\|Au - b\|_2^2$ with β , θ and μ as their respective control parameters.

The constrained equation (15) can be solved utilising Augmented Lagrangian technique iteratively by solving these equations:

$$(w_{k+1}, u_{k+1}, x_{k+1}) = \underset{w, u, x}{\operatorname{argmin}} \mathcal{L}_A(w, u, x). \quad (17)$$

$$\begin{cases} v_{k+1} = v_k - \beta(\mathcal{D}u_{k+1} - w_{k+1}) \\ \gamma_{k+1} = \gamma_k - \theta(u_{k+1} - x_{k+1}) \\ \lambda_{k+1} = \lambda_k - \mu(Au_{k+1} - b) \end{cases} \quad (18)$$

where, k represents the number of iterations and v , γ , λ are Lagrangian functions for $\mathcal{D}u = w$, $u = x$, $Au = b$ respectively. As it is hard to solve directly the three quadratic penalty terms efficiently, therefore, these are solved and employed by direction technique referred by [15], which alternatively minimises one variable while fixing the other variable. Equation (17) is split into three sub problems w , u and x and solved as referred in [3].

4.2 Restricted group sparse representation: phase 2

Since method of GSR [22] improves the PSNR performance, but is sensitive to over smoothing of images, therefore, in this paper it is proposed to use the hierarchical pyramid based fast GP-RCoS method as the initial phase of the GSR in place of multihypothesis (MH) predictions [19]. In the proposed work, maximum number of iterations in the GSR stage is restricted to 25 because most of the recovered test images achieve maximum PSNR level within 25 iterations. Thus, it is called as Restricted GSR phase. It has been verified empirically on 4 test images. Figure 7 shows the PSNR plot for different iteration counts for sampling ratio of 0.4. It can be clearly observed that GSR stage attains maximum (or near to maximum) PSNR value of test images in less than 25 iterations. Thus, the restricted iteration counts are set to 25 for GSR stage in the proposed work.

4.2.1 Restricted BCS-GSR algorithm

For performance improvement and fast convergence implementation, Split Bregman Iteration (SBI) [14,15] based restricted BCS-GSR decoder is used in this paper. This method addressed non-local sparsity using group based representation.

The image x of size N is divided into n overlapped patches of size $\sqrt{B_s}$. For every patch x_k ($k = 1, 2, \dots, n$), a searching window looks for its C best matched patches. The Group formation searches the similar patches based on Euclidean distance d over the search window S_g . Then, all matched similar patches are used to form a group matrix $x_{G_k} = \{x_{G_k}, x_{G_k}, \dots, x_{G_k}\}$. Here n is the number of image patches and the term x_{G_k} is called as Group. The reconstruction problem from x_{G_k} to x can be reformulated by averaging the group and the recovery can be done as;

$$x = \sum_{k=1}^n R_{G_k}^T (x_{G_k}) \cdot / \sum_{k=1}^n R_{G_k}^T (1_{B_s \times C}) \quad (19)$$

where R_{G_k} is an operator used for extracting of group x_{G_k} from x , $R_{G_k}^T$ is its transpose, $/$ represents element-wise division operation and $1_{B_s \times C}$ is an all-ones matrix with size $B_s \times C$.

The structure of split Bregman iteration (SBI) is used to iteratively solve the complex GSR regularisation-based image restoration process with subproblems as u subproblem [22]. On the basis of referred GSR modelling and recovery algorithm in [22], our modified restricted GSR algorithm is given as:

Algorithm 2 Restricted GSR for colour CIELAB images

1. Initialize : initial input as x_{org} as CIELAB image , $x = X_i^{LAB}$ where $i=1,2,3$
 2. If $i=1$ then $x = X_1^{LAB} = X_{Rec}^{GP-RCOS}$ is reconstructed L component of GP-RCoS phase.
else
 $x = X_i^{LAB} = x_{org} (i)$
end
 3. Set \leftarrow parameters λ , factor F , μ and Block size B
 Find parameter for hard threshold $\tau = \lambda * F / \mu \rightarrow Th = \sqrt{2 * \tau}$
 4. Input: measurement vector y and $\phi = A$,
 5. Do \leftarrow SBI till Iterations count \leftarrow BCS-GSR-SBI-Decoding
 Update $\hat{u} = u - \eta(\phi^T \phi u - \phi^T y + \mu(u - D_G^\circ \alpha_G - b))$
 Update $\hat{\alpha}_{G_k} = hard(\gamma_{r_{G_k}}, \sqrt{2\tau}) = \gamma_{r_{G_k}} \odot 1(abs(\gamma_{r_{G_k}}) - \sqrt{2\tau})$
 Update $b^{t+1} = b^t - (u^{t+1} - Gv^{t+1})$
 6. Evaluate PSNR \rightarrow end
-

4.3 Flow chart of the proposed HRCoGSR method

The sequential flow chart of the proposed HRCoGSR method is shown in Figure 8.

Figure 7 Validation of restricted iterations of GSR algorithm (see online version for colours)

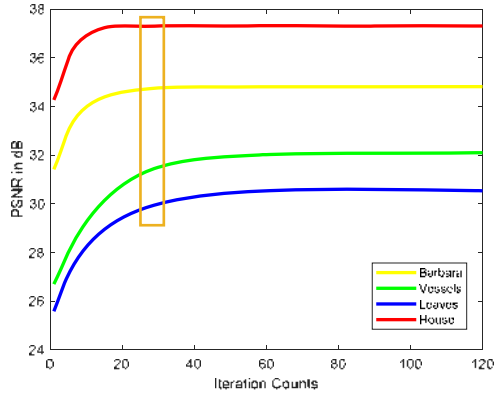
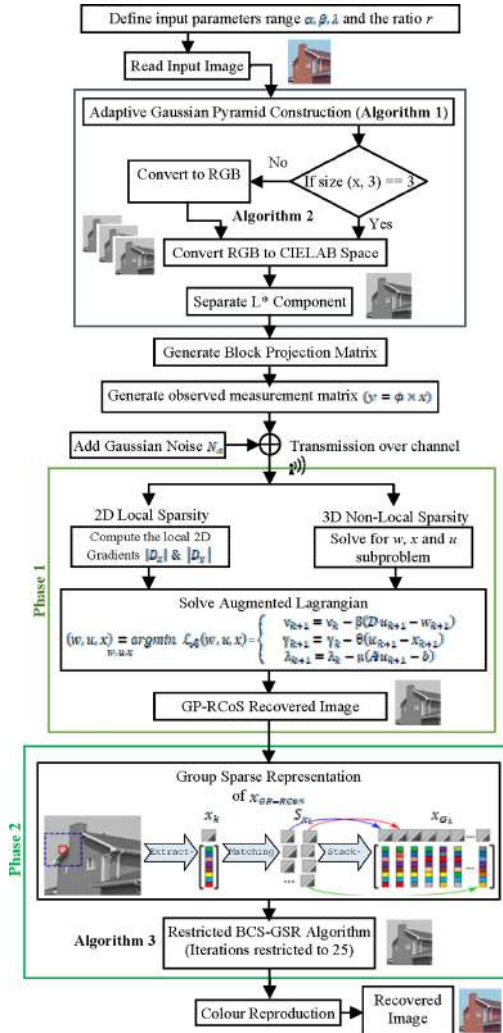


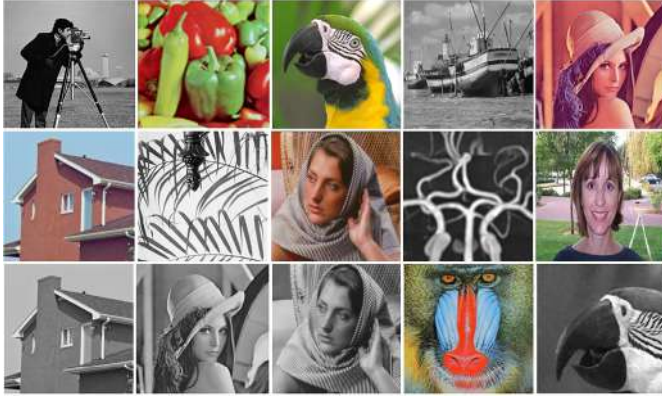
Figure 8 Flow chart of the proposed HRCoGSR method (see online version for colours)



5 Results and discussion

The performance of the proposed hierarchical pyramid based hybrid CS method is evaluated using the standard image database of 15 unique images as shown in Figure 9. The database consists of 2D (grey) and 3D (colour) images of varying sizes. Cameraman, boat, leaves are grey images of size 256×256 and vessels image is a grey image of size 112×112 . Peppers, Barbara, Parrot, Lena are colour images of size 256×256 while face image is of 512×512 size.

Figure 9 Sample database of grey/colour images of varying size for evaluation (see online version for colours)



All the simulations are performed in MATLAB 2013a on an Intel Core i3-5015U Dell system (2.10 GHz, 4 GB RAM) with Windows 10 Pro Operating System. Various experimentations were carried out and on the basis of empirical study, the proposed research methodology is defined and developed. The basic experimentation was started by validating the standard RCoS [3] based CS method. The first problem statement which is considered is speed improvement of RCoS method. Thus, it is proposed to use the hierarchical Gaussian Pyramid (GP) based approach (GP-RCoS) and speed up the execution process as explained in previous sections.

The design parameters B , B_s , L , C , μ , λ , θ and β are varied and optimally initialised for implementing GP-RCoS based recovery. The simulation and optimisation parameters are given in Table 2. The block size B for BCS is set to 32. For result execution λ is set to 12, $\beta = 7$, and $\theta = 3$. During non-local patch based similarity searching, block B_s is set as 8×8 local window $L = 41 \times 41$ and the best matched blocks C are set to be 10 [3]. For the GSR phase (Phase-2), number of iterations for the image recovery is restricted to 25 only.

5.1 Parametric performance evaluation of the proposed HRCoGSR method

The parametric performance of the proposed HRCoGSR CS methodology is being compared with the state of art existing CS based approaches. The prime concern of the research work is to improve the efficiency of collaborative sparse compressive sensing technique. Therefore, the proposed hybrid HRCoGSR is compared with existing RCoS

[3] method. Additionally, three GSR based compression and recovery methodologies viz. GSR [22], GSR-NCR [23] and HNLSR [35] have also been considered for comparative evaluation.

Table 2 Simulation and optimisation parameters for CS modelling

<i>S. No.</i>	<i>Parameters</i>	<i>Range</i>
1	μ (mu)	2^8
2	β (beta)	5–7
3	ε (tolerance)	1e–3
4	Maximum number of iterations in GP-RCoS	400
5	θ (theta)	2–3
6	B (Block Size for CS)	32
7	r (ratio/sample measurements)	{0.1–0.4}
8	S (Size of input image)	$\max [x_{\text{row}}, y_{\text{col}}]$

First goal of the paper was to design fast image recovery method, thus the computational time of the proposed method is compared with three existing methods. Total elapsed time for Vessels, Parrot and House grey images in TIFF format is evaluated and compared in Table 3.

Table 3 Computational time (in seconds) for different sampling ratios/measurements

<i>Images</i>	<i>Ratio (r)</i>	<i>RCoS</i>	<i>GSR</i>	<i>Proposed HRCoGSR method</i>
Vessels image of size 96×96	0.1	999.76	855.38	1102.60
	0.2	1188.58	820.14	1152.72
	0.3	703.78	866.20	802.07
	0.4	446.57	808.78	629.44
Parrot image of size 256×256	0.1	3937.54	3419.55	2076.17
	0.2	3513.03	3264.89	2095.04
	0.3	2953.46	1088.23	1234.56
	0.4	3165.91	1140.47	1183.62
House image of size 256×256	0.1	7683.10	6022.14	1296.22
	0.2	4557.54	3987.62	996.82
	0.3	3250.89	3106.56	968.1
	0.4	6142.49	3873.38	623.99
Average time		3211.89	2437.78	1180.113

The elapsed time comparison (in seconds) is presented in Table 3 for different sampling ratios from 0.1 to 0.4. The execution time is calculated on an Intel Core i3-5015U Dell system (2.10 GHz, 4 GB RAM) with Windows 10 Pro Operating System. This data may vary as per the system configuration. It can be observed from Table 3 that HRCoGSR method offers significant reduction in elapsed time for higher size images viz. Parrot &

House of size 256×256 . The proposed method takes additional 25 iterations of GSR thus it has slight increased computational time for small size Vessels image (96×96) at $r = 0.1$ and $r = 0.2$. The proposed method HRCoGSR offers almost 1/3rd average time than the customary RCoS approach.

The average elapsed time plot of the proposed method and existing methods is shown in Figure 10 for sampling ratios 0.1, 0.2, 0.3 and 0.4. It is evident from the plot that the proposed HRCoGSR method takes less computational time as compared with RCoS and GSR methods. The lowest execution time is marked by an orange circle in the plot.

Figure 10 Average elapsed time comparison plot (see online version for colours)

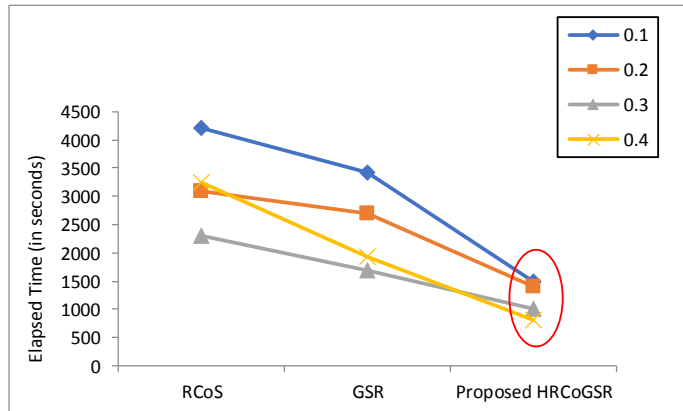
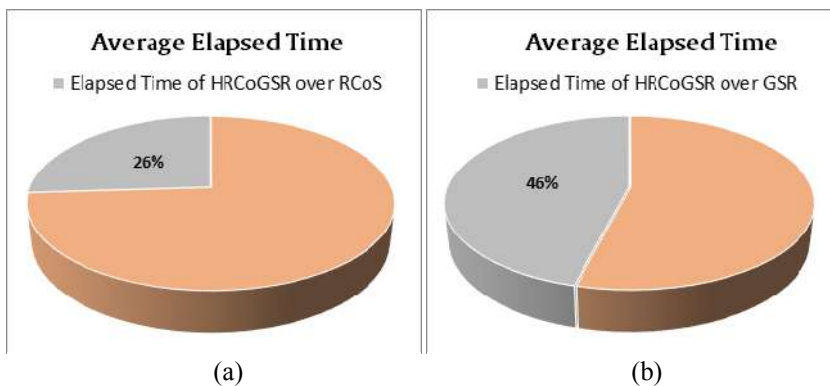


Figure 11 also illustrates the average elapsed time taken by the proposed method

- a over RCoS
- b over GSR method.

It is clear from Figure 11 that proposed HRCoGSR method takes around only 26% of the execution time over traditional RCoS method, saving 76% of time and it takes 46% of execution time over GSR, saving around 54% of time. A significant reduction in computational time is noticed which justifies the fast speed of the proposed method.

Figure 11 Average elapsed time taken by the proposed method: (a) over RCoS and (b) over GSR method (see online version for colours)



For quantitative performance evaluation of the proposed method, PSNR performance of 8 state-of-the-art existing CS based recovery methods are compared for different sampling ratios (r) from 0.1 to 0.4 for 9 images of different sizes. This comparison is presented in Table 4.

Table 4 PSNR performance comparisons of the proposed method with several state-of-the-art methods

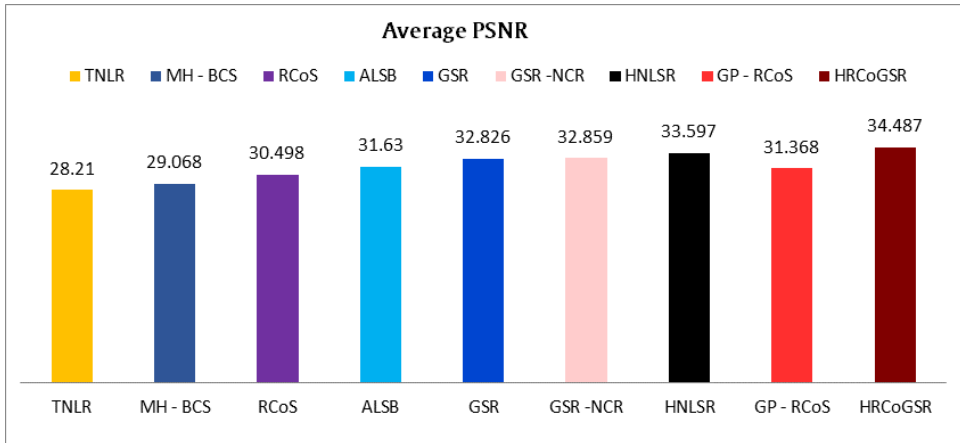
Images	Ratio (r)	PSNR in dB								
		TNLR [11]	MH-BCS [19]	RCoS [3]	ALSB [6]	GSR [22]	GSR-NCR [23]	HNLSR [35]	GP-RCoS (Phase-1 of HRCoGSR)	Proposed HRCoGSR
Cameraman 256×256	0.1	23.08	22.73	24.38	22.97	22.89	22.50	24.67	26.98	28.66
	0.2	25.77	25.88	27.97	26.65	27.17	26.30	28.34	30.75	32.77
	0.3	27.71	27.92	30.02	29.05	29.62	29.37	30.21	34.02	36.32
	0.4	29.48	29.36	31.76	31.01	31.64	31.59	33.25	37.01	38.58
Lena RGB 256×256	0.1	28.56	26.30	25.56	27.04	27.56	27.02	28.04	27.84	28.84
	0.2	31.04	29.81	29.60	30.72	31.36	30.87	31.57	31.65	33.92
	0.3	32.97	31.99	32.53	33.30	34.17	33.94	34.27	34.60	37.43
	0.4	34.86	33.80	34.29	37.41	36.48	36.46	36.82	36.40	39.89
Vessels 112×112	0.1	19.86	20.13	21.50	22.7	24.72	22.56	24.66	25.36	28.52
	0.2	22.60	25.12	27.29	30.8	33.07	30.64	33.16	30.26	37.15
	0.3	27.02	29.31	30/10	34.89	37.26	37.59	37.67	35.31	42.07
	0.4	30.75	33.44	35.66	37.96	40.52	40.90	40.62	38.62	44.91
Parrots RGB 256×256	0.1	24.76	25.30	25.55	26.03	26.37	26.05	27.22	26.68	27.76
	0.2	28.12	28.28	28.51	29.73	31.17	30.18	31.41	29.90	31.06
	0.3	30.82	30.16	30.79	31.98	33.81	33.07	33.83	33.47	37.26
	0.4	32.23	33.55	32.89	34.90	36.51	36.37	36.19	33.67	38.12
Leaves 256×256	0.1	19.43	20.52	22.40	21.32	23.30	22.66	24.54	19.03	20.23
	0.2	23.63	24.77	27.39	26.97	30.60	29.03	30.97	23.90	26.85
	0.3	27.18	27.70	30.87	31.01	34.46	34.89	34.54	27.23	30.93
	0.4	29.53	29.87	33.80	35.15	37.63	38.55	38.01	29.78	34.54
House RGB 256×256	0.1	29.71	30.32	33.45	32.18	33.46	32.35	33.58	31.19	34.77
	0.2	32.98	33.85	35.26	35.93	37.03	36.57	36.98	37.16	40.13
	0.3	35.22	35.69	36.30	38.36	38.32	39.37	40.16	40.25	42.79
	0.4	37.00	36.64	38.42	40.06	40.89	41.11	41.87	42.04	44.84
Boat image 256×256	0.1	25.67	26.09	27.85	27.75	28.37	27.62	28.56	25.48	26.64
	0.2	28.36	29.92	31.42	33.04	33.34	33.30	33.96	27.68	29.15
	0.3	30.79	32.26	34.32	36.45	36.30	37.26	37.22	31.90	34.31
	0.4	31.81	34.22	36.58	37.81	38.12	39.06	38.91	34.05	36.92

Table 4 PSNR performance comparisons of the proposed method with several state-of-the-art methods (continued)

Images	Ratio (<i>r</i>)	PSNR in dB								
		MH –				GSR –		HNLSR	GP–RCoS (Phase-1 of HRCoGSR)	Proposed HRCoGSR
		TNLR [11]	BCS [19]	RCoS [3]	ALSB [6]	GSR [22]	NCR [23]			
Barbara RGB 256×256	0.1	20.75	26.74	23.73	27.01	28.20	28.28	28.77	25.89	28.18
	0.2	22.34	30.81	26.6	31.77	34.69	33.91	33.89	29.62	33.65
	0.3	23.77	32.99	29.49	34.70	36.92	37.16	36.94	32.54	37.14
	0.4	25.65	35.12	32.76	37.23	38.99	39.22	39.16	34.82	39.74
Peppers 512×512	0.1	26.23	25.00	27.01	26.60	26.01	26.37	27.91	25.55	26.87
	0.2	29.35	28.45	30.87	29.87	30.83	30.46	31.19	30.62	33.87
	0.3	31.56	30.30	32.65	32.13	33.02	32.86	33.18	33.62	36.75
	0.4	35.06	34.46	36.37	36.23	37.21	37.32	37.87	36.69	39.99
Average		28.21	29.06	30.49	31.63	32.82	32.85	33.59	31.36	34.48

The average PSNR values are calculated for 9 different grey/colour images for evaluation. It is also shown graphically in Figure 12. It is clearly observed from Figure 12 that proposed HRCoGSR method offers around 4 dB average gain over RCoS method, 1.66 dB average gain over GSR and around 0.9 dB gain over HNLSR [35] method.

Figure 12 Comparison of average PSNR values (in dB) of the proposed method with existing CS methods (see online version for colours)



Average PSNR performance plots for different values of sampling ratios (*r*) are shown in Figure 13. It has been observed that for different values of sampling ratios (*r*), the proposed HRCoGSR method outperforms other techniques. From Figure 13, it is also clear that for higher value of *r*, the average PSNR value increases.

Figure 13 Comparison of average PSNR vs sampling ratio (r) for 9 different methods (see online version for colours)

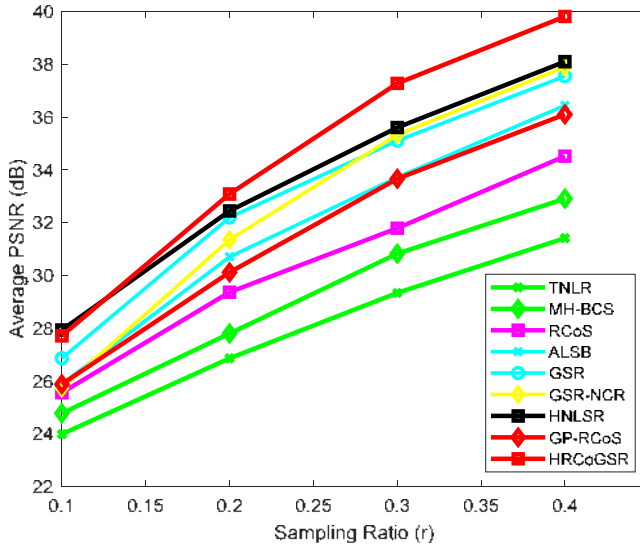
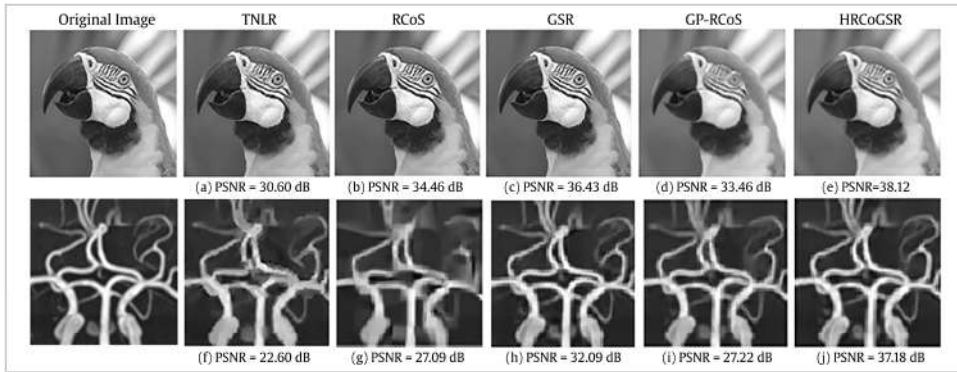


Figure 14 depicts the recovered images using the existing standard methods and the proposed CS method. Top row (a)–(e) shows the recovered Parrot image of size 256×256 for sampling ratio (r) = 0.4 and bottom row (f)–(j) shows the recovered Vessels image of size 96×96 for sampling ratio (r) = 0.2.

Figure 14 Recovered images using existing and proposed CS methods: (a)–(e) Recovered Parrot image of size 256×256 for sampling ratio, $r = 0.4$, (f)–(j) recovered vessels image of size 96×96 for sampling ratio, $r = 0.2$



Various parametric visualisations are plotted for the proposed method of HRCoGSR in Figure 15. Figure 15(a)–(c) represent the PSNR performance vs Iteration Counts plotted for different sampling ratios (from 0.1 to 0.4) for House, Cameraman and Parrot images. Figure 15(d)–(f) show the associated graph drawn between the Iteration Counts and sampling ratio (r). A comprehensible observation can be seen from these plots that, as the sampling ratio increases, lesser number of iterations are required to attain enhanced PSNR values. Consequently, the method will terminate faster leading to less

computational time. It demonstrates that the HRCoGSR method has an excellent convergence property.

Figure 15 (a)–(c) PSNR performance calculation with respect to iteration counts for different sampling ratios (r). (d)–(f) are associated graph drawn between the iteration counts and sampling ratio (r) (see online version for colours)

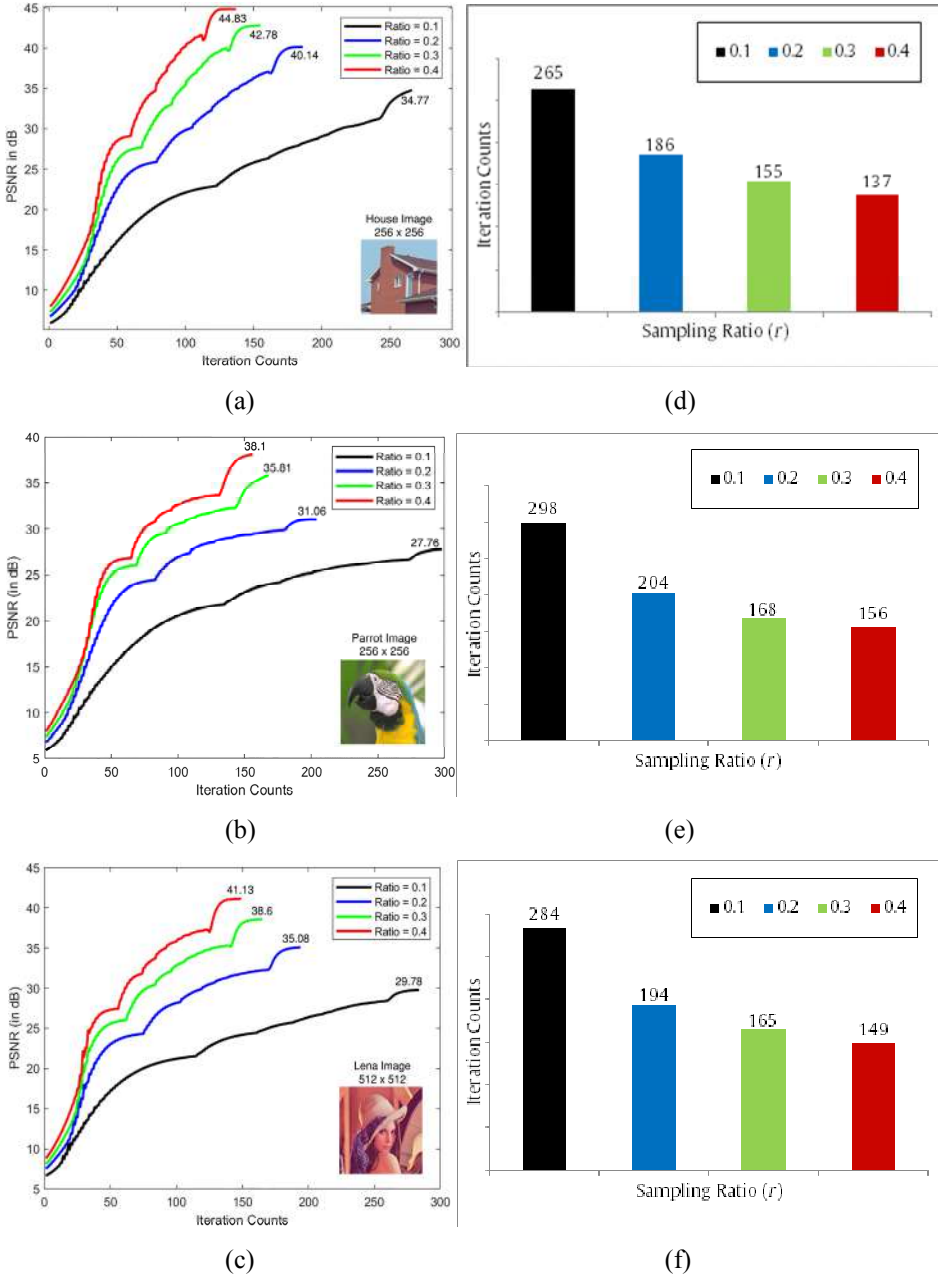
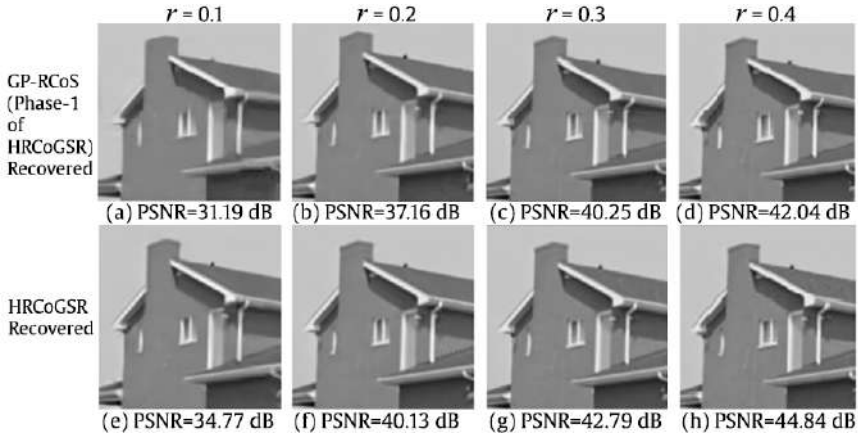


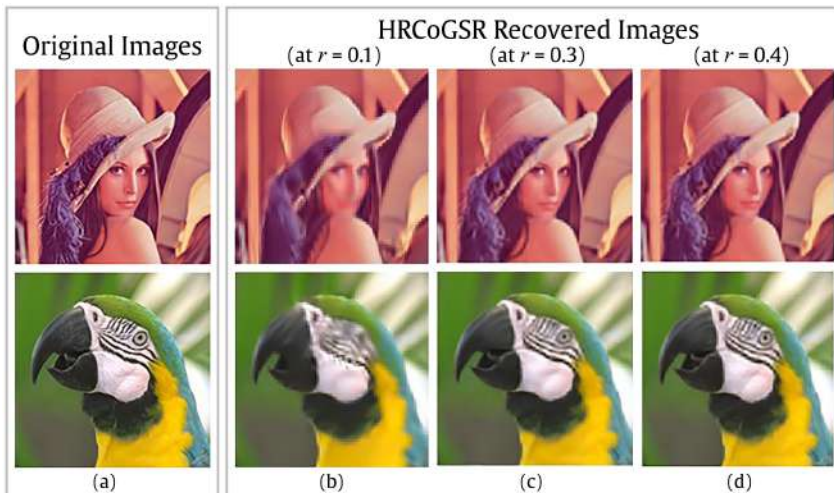
Figure 16(a)–(d) shows the recovered House images of size 256×256 at GP-RCoS Phase (Phase-1 of HRCOGSR) and Figure 16(e)–(h) are the final recovered images of the proposed HRCoGSR method for different values of r (0.1–0.4).

Figure 16 Recovered House image (256×256) for GP-RCoS (a)-(d) and HRCoGSR (e)-(h) proposed method with different sampling ratios ($r = 0.1 - 0.4$)



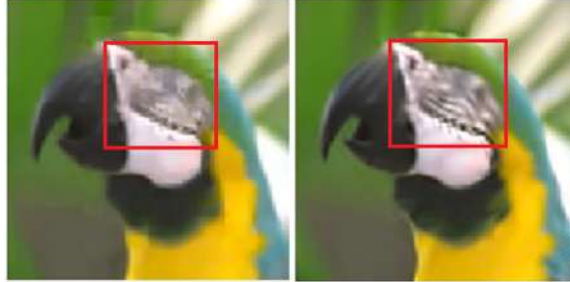
Colour image recovery results of the proposed method are shown in Figure 17 for lower as well as higher sampling ratio/sample measurements. In Figure 17, first column images (a) are original images, second column images (b) are recovered images at lower ratio $r = 0.1$, third and fourth column images (c)-(d) are recovered images at higher ratio $r = 0.3$ and $r = 0.4$ respectively. PSNR for the recovered image Lena by HRCoGSR method is 28.84 dB (for $r = 0.1$), 37.43 dB (for $r = 0.3$) and 39.89 dB (for $r = 0.4$).

Figure 17 Performance comparison of the colour image recovery with proposed HRCoGSR method for lower sampling ratio (at $r = 0.1$) and higher sampling ratio (at $r = 0.3$ and 0.4) (see online version for colours)



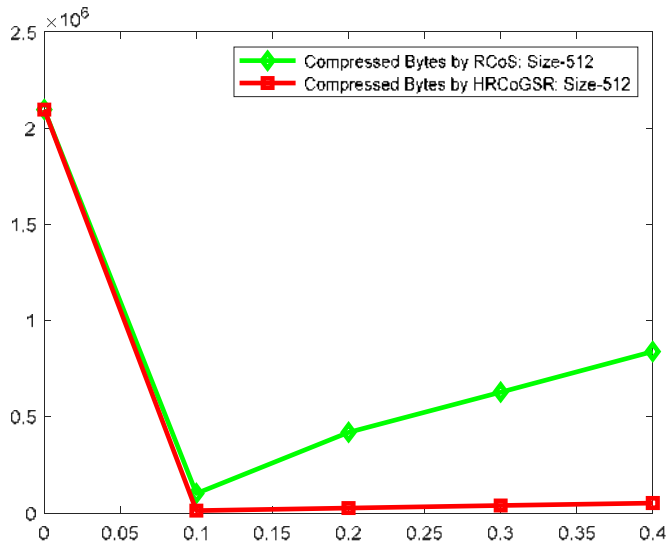
The reproduction efficiency of the proposed colour image CS methods over standard RCoS method is clearly seen in Figure 18. Improvements in terms of sparsity limitation of RCoS with proposed methods are shown by red squares in Figure 18 for the image recovery at low value of ratio ($r = 0.2$).

Figure 18 Comparative results for Parrot image at lower sampling ratio ($r = 0.2$) for improvement in sparsity limitation: (a) RCoS recovered and (b) HRCoGSR recovered (see online version for colours)



The compression achieved by the standard RCoS method and the proposed HRCoGSR method can be quantified by the number of utilised bytes. Figure 19 illustrates the comparison of the compression achieved in terms of the number of bytes used for a 512×512 House image at different sampling ratios ($r = 0.1-0.4$). The first value is representing the size of original input image in bytes and further values are plotted for sampling ratios 0.1, 0.2, 0.3 and 0.4. It can be observed that the proposed method significantly reduces the number of bytes utilised and offers higher compression as compared to the baseline method RCoS.

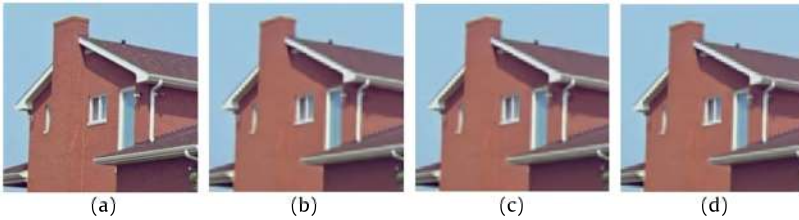
Figure 19 Comparison of the compression achieved in terms of the number of bytes used for a 512×512 image (see online version for colours)



5.2 Performance under noise attacks

The performance of the proposed method is also evaluated under the presence of additive Gaussian noise. The measurement matrix is added with a noise of 100, 150 and 250 dB SNR. Reconstructed image results of the proposed HRCoGSR method for House image are presented in Figure 20 for measurements/sampling ratio of 0.2 (20%). It is observed that proposed method significantly recovers the image even at higher noisy environment. Less reduction in PSNR performance is noticed under noise attack.

Figure 20 Result of the proposed method under AWGN noise attack over measurement matrix: (a) original image; (b) 100 dB Noise, PSNR = 40.123 dB; (c) 150 dB Noise, PSNR = 40.113 and (d) 250 dB Noise, PSNR = 40.09 (see online version for colours)



6 Conclusion

This paper proposed a fast and efficient hierarchical pyramid based colour image compressive sensing method (HRCoGSR) characterising and utilising both local and non-local similarities. At the front-end, a dimension adaptive pyramid based GP-RCoS method is designed for BCS based reconstruction which can adopt both grey and colour images. In the second phase, the GP-RCoS reconstructed image is used as the initial estimate for the restricted GSR based recovery. The proposed methods combined the benefits of patch and group based compressive sensing approaches by designing hybrid combination of RCoS and GSR methods.

As an experiment, URD and ONRD based projection matrices are also generated and compared. PSNR results show that ONRD based projection matrix method yields higher PSNR values as compared with URD method.

Simulation of the proposed HRCoGSR method along with seven existing standard methods is carried out for variety of standard grey and colour images for different sampling ratios (r) in MATLAB 2013a. Results show that the proposed HRCoGSR method is highly efficient and much faster than existing methods. The average elapsed time taken by the proposed HRCoGSR method is only 26% of that of the standard RCoS method, saving 74% computational time. When compared to GSR method, the proposed method takes only 46% of the average computational time calculated for Intel Core i3-5015U Dell (2.10 GHz, 4 GB RAM) system. The initial phase of pyramid construction based GP-RCoS method alone offers better PSNR than early CS methods like TNLr, MH, and RCoS. The performance results for Parrot, Lena, Barbara, Peppers and House colour images are improved specifically. The PSNR performance of House image has increased from 38.42 dB to 42.04 dB with an increment of around 8% in GP-RCoS phase only.

In order to minimise the blurriness offered by the initial phase of GP-RCoS, the results are fed to restricted GSR phase. The final results of the proposed HRCoGSR method offers around 4 dB average gains over RCoS, 1.66 dB average gain over GSR, around 0.9 dB gain over HNLSR methods. Several parametric performance plots are presented which clearly justify the effectiveness and performance improvement offered by proposed method over other existing methods in terms of compression, computational time and PSNR performance. However, the perceptual quality of the bigger size images needs further improvement, as the reconstructed image seems to be over-smoothened.

The proposed work is applicable in all the sectors of imaging where taking samples is complex and costly. It can be used in efficient image acquisition, low-powered sensing of images and distributed camera sensor network applications.

Future scope comprises the expansion of HRCoGSR in applications like image deblurring, image denoising etc. Local sparsity constraints can be tackled for completely removing the over smoothing effects. Use of multiple dictionaries can also improve the performance further.

References

- 1 Candes, E.J. and Wakin, M.B. (2008) 'Wakin, M.B.: An introduction to compressive sampling', *IEEE Signal Process Mag.*, Vol. 25, No. 2, pp.21–30.
- 2 Mun, S. and Fowler, J.E. (2009) 'Block compressed sensing of images using directional transforms', *Proceedings – International Conference on Image Processing, ICIP*, Cairo, Egypt, pp.3021–3024.
- 3 Zhang, J., Zhao, D., Zhao, C., Xiong, R., Ma, S. and Gao, W. (2012) 'Image compressive sensing recovery via collaborative sparsity', *IEEE J. Emerg. Sel. Topics Power Electron.*, Vol. 2, No. 3, pp.380–391.
- 4 He, L. and Carin, L. (2009) 'Exploiting structure in wavelet-based bayesian compressive sensing', *IEEE Trans. Signal Process.*, Vol. 57, No. 9, pp.3488–3497.
- 5 He, L., Chen, H. and Carin, L. (2010) 'Tree-structured compressive sensing with variational bayesian analysis', *IEEE Signal Process Lett.*, Vol. 17, No. 3, pp.233–236.
- 6 Zhang, J., Zhao, C., Zhao, D. and Gao, W. (2014) 'Image compressive sensing recovery using adaptively learned sparsifying basis via L0 minimization', *Signal Process.*, Vol. 103, pp.114–126.
- 7 Haupt, J. and Nowak, R. (2006) 'Signal reconstruction from noisy random projections', *IEEE Trans. Inf. Theory*, Vol. 52, No. 9, pp.4036–4048.
- 8 Bertero, M. and Boccacci, P. (2020) *Introduction to Inverse Problems in Imaging, Introduction to Inverse Problems in Imaging*, CRC Press, Boca Raton, Florida, USA.
- 9 Li, C., Yin, W. and Zhang, Y. (2009) *User's Guide for TVAL 3: TV Minimization by Augmented Lagrangian and Alternating Direction Algorithms*, CAAM Report, Vol. 20.
- 10 Li, C., Yin, W., Jiang, H. and Zhang, Y. (2013) 'An efficient augmented lagrangian method with applications to total variation minimization', *Comput. Optim. Appl.*, Vol. 56, No. 3, pp.507–530.
- 11 Zhang, J., Liu, S., Xiong, R., Ma, S. and Zhao, D. (2013) 'Improved total variation based image compressive sensing recovery by nonlocal regularization', *Proceedings – IEEE International Symposium on Circuits and Systems*, Beijing, China, pp.2836–2839.
- 12 Nocedal, J. and Wright, S. (2006) *Numerical Optimization, Series in Operations Research and Financial Engineering*, Springer, New York, USA.

- 13 Afonso, M.V., Bioucas-Dias, J.M. and Figueiredo, M.A.T. (2010) 'Fast image recovery using variable splitting and constrained optimization', *IEEE Trans. Image Process.*, Vol. 19, No. 9, pp.2345–2356.
- 14 Goldstein, T. and Osher, S. (2009) 'The split bregman method for L1-regularized problems', *SIAM J. Imaging Sci.*, Vol. 2, No. 2, pp.323–343.
- 15 Cai, J.F., Osher, S. and Shen, Z. (2009) 'Split bregman methods and frame based image restoration', *Multiscale Model. Simul.*, Vol. 8, No. 2, pp.337–369.
- 16 Chen, G., Zhang, J. and Li, D. (2016) 'Fractional-order total variation combined with sparsifying transforms for compressive sensing sparse image reconstruction', *J. Vis. Commun. Image Represent.*, Vol. 38, pp.407–422.
- 17 Zhong, Y., Zhang, J., Cheng, X., Huang, G., Zhou, Z. and Huang, Z. (2019) 'Reconstruction for block-based compressive sensing of image with reweighted double sparse constraint', *EURASIP J. Image Video Process.*, Vol. 2019, No. 63, pp.1–14.
- 18 Zhang, J., Zhao, D., Jiang, F. and Gao, W. (2013) 'Structural group sparse representation for image compressive sensing recovery', *Data Compression Conference Proceedings*, Snowbird, Utah, USA, pp.331–340.
- 19 Chen, C., Tramel, E.W. and Fowler, J.E. (2011) 'Compressed-sensing recovery of images and video using multihypothesis predictions', *Conference Record – Asilomar Conference on Signals, Systems and Computers*, Pacific Grove, California, pp.1193–1198.
- 20 Tramel, E.W. and Fowler, J.E. (2011) 'Video compressed sensing with multihypothesis', *Data Compression Conference Proceedings*, Snowbird, Utah, USA, pp.193–202.
- 21 Chen, J., Chen, Y., Qin, D. and Kuo, Y. (2015) 'An elastic net-based hybrid hypothesis method for compressed video sensing', *Multimed. Tools. Appl.*, Vol. 74, No. 6, pp.2085–2108.
- 22 Zhang, J., Zhao, D. and Gao, W. (2014) 'Group-based sparse representation for image restoration', *IEEE Trans. Image Process.*, Vol. 23, No. 8, pp.3336–3351.
- 23 Shi, W., Chen, C., Jiang, F., Zhao, D. and Shen, W. (2016) 'Group-based sparse representation for low lighting image enhancement', *Proceedings – International Conference on Image Processing, ICIP*, Phoenix, Arizona, USA, pp.4082–4086.
- 24 Li, X., Shen, H., Li, H. and Zhang, L. (2016) 'Patch matching-based multitemporal group sparse representation for the missing information reconstruction of remote-sensing images', *IEEE J. Sel. Top. Appl. Earth Obs. Remote Sens.*, Vol. 9, No. 8, pp.3629–3641.
- 25 Xu, J., Qiao, Y., Fu, Z. and Wen, Q. (2019) 'Image block compressive sensing reconstruction via group-based sparse representation and nonlocal total variation', *Circuits, Systems, and Signal Processing*, Vol. 38, No. 1, pp.304–328.
- 26 Xie, Z., Liu, L. and Yang, C. (2019) 'An entropy-based algorithm with nonlocal residual learning for image compressive sensing recovery', *Entropy*, Vol. 21, No. 9, p.900.
- 27 Li, Y., Liu, L., Zhao, Y., Cheng, X. and Gui, G. (2020) 'Nonconvex nonsmooth low-rank minimization for generalized image compressed sensing via group sparse representation', *J. Franklin Inst.*, Vol. 357, No. 10, pp.6370–6405.
- 28 Zha, Z., Yuan, X., Wen, B., Zhou, J. and Zhu, C. (2018) 'Joint patch-group based sparse representation for image inpainting', in Zhu, J. and Takeuchi, I. (Eds.): *Proceedings of Machine Learning Research 95*, Vol. 95, PMLR, pp.145–160.
- 29 Zha, Z., Yuan, X., Wen, B., Zhang, J., Zhou, J. and Zhu, C. (2020) 'Image restoration using joint patch-group-based sparse representation', *IEEE Trans. Image Process.*, Vol. 29, pp.7735–7750.
- 30 Takeda, H., Farsiu, S. and Milanfar, P. (2007) 'Kernel regression for image processing and reconstruction', *IEEE Trans. Image Process.*, Vol. 16, No. 2, pp.349–366.
- 31 Shi, Y., Zhu, X.X. and Bamler, R. (2019) 'Nonlocal compressive sensing-based SAR tomography', *IEEE Trans Geosci Remote Sens.*, Vol. 57, No. 5, pp.3015–3024.
- 32 Zammit, J. and Wassell, I.J. (2020) 'Adaptive block compressive sensing: toward a real-time and low-complexity implementation', *IEEE Access*, Vol. 8, pp.120999–121013.

- 33 Sun, Y., Zhang, Z., Jiang, W., Zhang, Z., Zhang, L., Yan, S. and Wang, M. (2020) 'Discriminative local sparse representation by robust adaptive dictionary pair learning', *IEEE Trans. Neural Netw. Learn. Syst.*, Vol. 31, No. 10, pp.4303–4317.
- 34 Erkoç, M.E. and Karaboğa, N. (2021) 'Sparse signal reconstruction by swarm intelligence algorithms', *Engineering Science and Technology, an International Journal*, Vol. 24, No. 2, pp.319–330.
- 35 Li, L., Xiao, S. and Zhao, Y. (2020) 'Image compressive sensing via hybrid nonlocal sparsity regularization', *Sensors (Switzerland)*, Vol. 20, No. 19, p.5666.
- 36 Jain, A., Swami, P.D. and Datar, A. (2022) 'Fast gaussian pyramid based recovery with collaborative sparsity for image compressive sensing', *2021 IEEE International Conference on Smart Technologies for Power, Energy and Control (STPEC)*, IEEE, Bilaspur, India, pp.1–6.
- 37 Placzek, B. (Ed.) (2022) *Data Acquisition – Recent Advances and Applications in Biomedical Engineering*, IntechOpen, London, <https://doi.org/10.5772/intechopen.87796>
- 38 Kakaraparty, K., Tasneem, N. and Mahbub, I. (2020) 'A low-power front-end with compressive sensing circuit for neural signal acquisition designed in 180 nm CMOS process', *Proceedings of the 2020 IEEE Dallas Circuits and Systems Conference, DCAS. 2020*, Dallas, USA, pp.1–5.
- 39 Zhang, Q., Li, B. and Shen, M. (2019) 'A novel compression method based on bandlet and compressive sensing for ultrasound image', *2019 IEEE 4th International Conference on Signal and Image Processing, ICSIP. 2019*, Southeast University (Wuxi), China, pp.985–988.
- 40 Luo, M.R. (2016) *CIELAB*. In: Luo, M.R. (Eds) *Encyclopedia of Color Science and Technology*, Springer, New York, NY, https://doi.org/10.1007/978-1-4419-8071-7_11